ACS OMEGA

http://pubs.acs.org/journal/acsodf

Article

Optically Clear Silk Fibroin Films with Tunable Properties for Potential Corneal Tissue Engineering Applications: A Process−Property−Function Relationship Study

Maya Beena, Jimna Mohamed Ameer, and Naresh Kasoju*

Cite This: *ACS Omega* 2022, 7, 29634−29646

Read Online

ACCESS | Metrics & More | Article Recommendations

ABSTRACT: Owing to the shortage of donor corneas and issues associated with conventional corneal transplantation, corneal tissue engineering has emerged as a promising therapeutic alternative. Biocompatibility and other attractive features make silk fibroin a biomaterial of choice for corneal tissue engineering applications. The current study presents three modes of silk fibroin film fabrication by solvent casting with popular solvents, viz. aqueous (aq), formic acid (FA), and hexafluoroisopropanol (HFIP), followed by three standard modes of postfabrication annealing with water vapor, methanol vapor, and steam, and systematic characterization studies including corneal cell culture *in vitro*. The results indicated that silk fibroin films made from aq, FA, and HFIP solvents had surface roughness (Rq) of 1.39, 0.32, and 0.13, contact angles of 73°, 85°, and 89°, water uptake% of 58, 29, and 27%, swelling ratios of 1.58, 1.3, and 1.28, and water vapor transmission% of 39, 26, and 22%, respectively. The degradation rate was in the order of aq > HF > FA, whereas the tensile strength was in the order of aq < HF < FA. Further, the results of the annealing process indicated notable changes in morpho-topographical, physical, degradation, and tensile properties. However, the films showed no detectable changes in chemical composition and remained optically clear with >90% transmission in the visible range, irrespective of fabrication and postfabrication processing conditions. The films were noncytotoxic against L929 cells and were cytocompatible with rabbit cornea-derived SIRC cells *in vitro*. The study demonstrated the potential of fine-tuning various properties of silk fibroin films by varying the fabrication and postfabrication processing conditions.

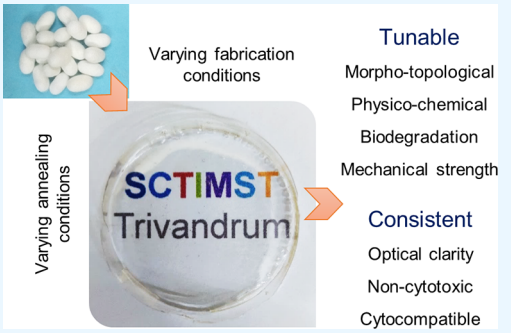

1. INTRODUCTION

Corneal tissue engineering is becoming an attractive therapeutic alternative toward corneal regeneration. Different biomaterials are being tested *in vitro*, *in vivo*, and in clinical studies; however, the loss of transparency and lack of strength are some of the bottlenecks in clinical success.[1] Efforts are made across the globe to find effective biomaterials for clinically compliant corneal equivalents. Among them, silk fibroin (SF)-based biomaterials are getting attention in recent times owing to the various advantages, viz. abundance availability, amenability of processing in aqueous and organic solvents, attractive chemistry for functionalization, ease of developing various forms of articles like films and porous sponges, proven biocompatibility with low immunogenic reaction, tunable mechanical and degradation properties, and excellent optical properties.[2−6] SF from *Bombyx mori* consists of three protein subunits, viz. a heavy chain of about 350 kDa, a light chain of about 26 kDa, and glycoprotein P25 of about 30 kDa.[7] The design feature of the silk domain includes N-terminal and C-terminal peptide domains with repetitive sequences in between. The central core of the SF sequence is composed of 12 repetitive hydrophobic regions made up of amino acids such as Gly-Ala-Gly-Ala-Gly-Ser/Tyr (GAGAGS/Y) and GAAS tetramers at the terminus and 11 interspersed amorphous regions rich in Gly. Apart from obtaining a pure form of SF with ease of processing, the abundant availability across various parts of the globe made SF a biomaterial of choice for various biomedical applications.[8]

SF can be fabricated into a variety of forms, viz. films, hydrogels, porous sponges, and micro/nanofibrous matrices.[2,9,10] Depending on the process, the parameters involved would strongly influence the properties of the resultant product. For instance, Tamada reported a new process of fabricating SF porous sponges by freeze-thawing of fibroin aqueous solution in the presence of a small amount of an organic solvent.[11] It was demonstrated that the solvent type, fibroin concentration, freezing temperature, and time influ-

Received: March 16, 2022
Accepted: August 5, 2022
Published: August 17, 2022

https://doi.org/10.1021/acsomega.2c01579
ACS Omega 2022, 7, 29634−29646

enced the sponge fabrication and its porosity as well as mechanical properties. In a similar study, Kasoju et al. reported the preparation of SF hydrogel by nonsolvent-induced phase separation.[12] It was described that the concentration of nonsolvent influenced the gelation time, pore properties, and secondary structural content of resultant SF hydrogel. Bray et al. evaluated silk films for use in repairing the cornea after injury due to their transparent nature and a high degree of biocompatibility.[13] They found excellent transmission % and transparency for silk films. Postfabrication processes are usually done to enhance the properties of resultant SF products. Typically, they are performed to modulate the β-sheet structure of silk in the products to fine-tune properties such as stiffness and degradation. It was reported that high β-sheet content provides high tensile strength and low degradation rate. For instance, Lu et al. performed postfabrication processing of silk films by methanol and water annealing and found that the methanol treatment induced more β-sheet formation and therefore reduced biodegradation of films.[14]

A tremendous amount of exploratory research was recorded in the literature in the field of silk-based biomaterials. Given their extraordinary properties as a biomaterial, the ease of processing, availability around the year, and relatively less expensive nature have made them a biomaterial of choice for many in the field in general. SF films can be readily made by a simple solvent casting approach. A range of studies have reported the preparation of SF films with a variety of process parameters; however, a systematic process−property−function relationship analysis comparing widely used solvents and annealing conditions could be interesting. To this end, we formulated the current study with a hypothesis that SF, when processed into films, following various fabrication and postfabrication treatments, shows variations in morpho-topological, physico-chemical, optical, and biological properties of SF films in the context of corneal tissue engineering. Accordingly, we designed the study involving three modes of fabrication by solvent casting with popular solvents, viz. aqueous (aq), formic acid (FA), and hexafluoroisopropanol (HFIP) solvents, followed by three popular modes of postfabrication annealing with water vapor (H_2O), methanol vapor (MeOH), and steam. We performed systematic characterization studies including cell culture studies with model corneal cells *in vitro* and investigated the process−property−function relationship.

2. MATERIALS AND METHODS

2.1. Materials. Domesticated *B. mori* silk cocoons were obtained from a local farmer based in Palakkad, Kerala, India. Lithium bromide, sodium carbonate, formic acid (≥96%), sodium azide, dialysis bag (molecular weight cut-off, 12−14 kDa), sodium hydroxide, paraformaldehyde, and protease (type XIV from *Streptomyces griseus*, ≥3.5 units/mg) were purchased from Sigma-Aldrich, India. 1,1,1,3,3,3-Hexafluoro-2-isopropanol (98%) and methanol were purchased from Spectrochem, India. Dulbecco's modified Eagle's medium (DMEM), fetal bovine serum, penicillin−streptomycin, trypsin, Alamar blue, Hoechst, and rhodamine-phalloidin were bought from Thermo Fisher, India. The MTT (3-(4,5-dimethylthiazol-2-yl)-2,5-diphenyltetrazolium) reagent and phosphate-buffered saline (PBS) powder were obtained from Hi-Media, India. L929 (mouse subcutaneous connective fibroblasts) cells were purchased from American Type Culture Collection, USA, and SIRC (Statens Serum Institut Rabbit Cornea) cells were obtained from National Centre for Cell Science, Pune, India.

2.2. Preparation of Silk Fibroin Films. The cocoons were processed to yield aqueous reconstituted SF as per Rockwood et al.[15] Briefly, to remove the sericin, 5 g of *B. mori* cocoons was degummed by boiling for 30 min in 2 L of 0.02 M sodium carbonate solution and then rinsed with ultrapure water several times. Subsequently, 2 g of degummed SF fibers was dissolved in 8 mL of 9.3 M lithium bromide solution set at 60 °C for 4 h. The mixture was then dialyzed against ultrapure water for 48 h with at least six intermittent water changes. The resultant solution was subjected to centrifugation (Hermle, Type Z326 K, Germany) at 5000 rpm for 15 min to remove any insoluble matter. The aqueous SF solution was either used as such for aqueous solvent-based processing of films or subjected to freeze-drying in a lyophilizer (Christ Alpha 1-4 LD, Germany) at −50 °C for 24 h to yield the SF sponge, which was then used for non-aqueous solvent-based processing of films.

Subsequently, SF films were fabricated by the solvent casting approach using three different solvents, viz. aq, HFIP, and FA solvents. For preparing aq films, after aqueous reconstitution, the concentration of SF solution was determined and adjusted to 5% (w/v). For preparing HFIP and FA films, the SF sponge, obtained after the lyophilization process, was dissolved in HFIP and FA solvents, respectively, to prepare a solution of 5% (w/v). Then, 2.5 mL of SF solution was poured into a clean 35 mm Petri dish and was kept in a 37 °C mini-incubator (Labnet, US) for overnight drying. After ensuring complete drying, SF films were further subjected to postfabrication processing, i.e., annealing in three different conditions, viz. water vapor (H_2O), methanol vapor (MeOH), and steam. For this purpose, the SF films were placed in a Petri dish kept inside a wide-mouth beaker filled with water or methanol. The chamber was tightly covered with a cling film to restrict vapors from escaping and kept in a mini-incubator set at 37 °C for 24 h. As for steam annealing, the films were autoclaved according to standard conditions. Subsequently, the SF films were carefully collected, air-dried, and stored in a desiccator until further characterization.

2.3. Characterization of Silk Fibroin Films. *2.3.1. Morpho-Topographical Properties.* The morphological features of SF films, prepared in three solvents and subjected to an annealing process in three environments, were analyzed through scanning electron microscopy (SEM, FEI Quanta 200). For this purpose, the films were first subjected to gold sputtering for 3 min at a voltage of 20 kV in a sputter coating machine (Hitachi E 101, Japan). Images at 5000× magnification were captured, where at least three samples were analyzed and a representative picture was presented. Further, to find the effect of process parameters on topographical properties in quantitative terms, we have performed surface profilometry of the films using a surface profilometer (Taylor Hobson Precision Talysurf CLI 1000). At least three samples were analyzed, and the root mean square roughness values (Rq) were presented as averaged values.

2.3.2. Physical Properties. Surface wettability is one of the important criteria for any biomaterial candidate. Typically, this is analyzed by contact angle measurement. In this study, static contact angles of SF films, processed under different fabrication and postfabrication conditions, were measured by the sessile drop method in a computer-controlled goniometer (OCA 20, Data Physics). Briefly, a droplet of 10 μL of distilled

https://doi.org/10.1021/acsomega.2c01579
ACS Omega 2022, 7, 29634−29646

water was dropped onto the surface of the sample, the image was captured within 5 s, and the contact angle was measured using the software supplied with the machine.

Apart from surface wettability properties, it is also important to assess how much water the SF films can hold, thereby how much they swell, and what are the effects of process parameters on such properties. For this purpose, SF films with predetermined weight were immersed in 5 mL of ultrapure water at 37 °C for 24 h. Subsequently, the films were collected and gently wiped with tissue paper and the wet weight of the films was measured. The water uptake capacity and swelling ratio were calculated as per eqs 1 and 2, respectively, wherein W_s denotes the swollen weight of the sample and W_d denotes the dry weight of the sample.

$$\text{water uptake (\%)} = \left[\frac{(W_s - W_d)}{W_s}\right] \times 100 \quad (1)$$

$$\text{swelling ratio} = \frac{W_s}{W_d} \quad (2)$$

Water vapor transmission (WVT) is another critical parameter for biomaterials. Here, the effect of process parameters on the WVT of SF films was analyzed as per earlier protocol with slight modification.[16] Briefly, SF films were cut out to fit into a vented cap of vials filled with 1 mL of water. The initial weight of the assembled vials was recorded, and then the setup was kept at 37 °C for 24 h. Vials fitted with a plastic film (OHP sheet) and vials with an open cap were considered as controls for comparison purposes. WVT was calculated as per eqs 3 and 4, where the area of the vent was 0.28 cm^2 and the time of the study was 24 h.

$$\text{WVT rate} = \frac{\text{initial weight} - \text{final weight}}{\text{area} \times \text{time}} \quad (3)$$

$$\text{WVT\%} = \left(\frac{\text{WVT of test film}}{\text{WVT of open system}}\right) \times 100 \quad (4)$$

2.3.3. Chemical/Structural Properties. To assess the effects of process parameters on chemical composition as well as structural features of SF films, we have performed Fourier transform infrared spectroscopy−attenuated total reflectance (ATR-FTIR) spectroscopy. For this purpose, the SF films prepared with different processing conditions were placed on the sample trough and scanned in the range of 4000 to 400 cm^{-1} wavenumber in an ATR-FTIR spectroscope (Nicolet 5700, Nicolet Inc., Madison, USA). The spectra were taken at a resolution of 1 cm^{-1}, and 32 scans per sample were evaluated. While the full spectrum was analyzed for potential changes in chemical composition due to processing, the spectrum from 1700 to 1600 cm^{-1} was analyzed to get insights into structural features. The spectra of degummed silk fiber and aqueous reconstituted SF were also recorded for comparison purposes.

2.3.4. Mechanical Properties. Silk materials are known for their tough mechanical properties. To understand the influence of fabrication and postfabrication processing, the SF films were subjected to tensile testing in a UTM Instron 3345 testing machine equipped with a 100 N capacity load cell and pneumatic clamps. For this purpose, the silk films were cast in a 90 mm Petri dish, and the films were subsequently cut into strips of 6 × 5 cm dimensions using a razor blade. Care was taken not to introduce any cracks along the edges while cutting the samples. Before testing, the films were hydrated in PBS for 10 min. They were blotted in-between tissue paper to remove excess water, and the samples were loaded onto the testing machine. A displacement control mode was used, with a crosshead displacement rate of 10 mm/min. The measured width of the gauge region of the slat was multiplied by the specimen thickness to convert load data to tensile stress values. The initial linear elastic modulus, elongation at break, and ultimate tensile strength were calculated from stress/strain plots.

2.3.5. Optical Properties. Optical clarity and transparency are the top most important qualifying criteria for any artificial or bioartificial corneal substitutes. The optical properties of SF films prepared by different processing conditions were determined by following three approaches: first, by visual inspection, second, by analyzing the absorbance spectra ranging from the UV spectrum to the visible spectrum, and third, by determining transmission (T%).

As for the absorption spectra and T%, SF films prepared by different processing conditions were cut out into 4 mm sizes and were placed into wells of 96-well plates. The absorbance spectrum was read for each sample in the UV−visible range from 200 to 700 nm in a multiwell plate reader (Biotech, USA). Subsequently, samples were wetted with 100 μL of ultrapure water and incubated at room temperature for 5 h. Water was removed from the wells completely, and the spectra were read again in the plate reader for the same spectral range. Subsequently, the absorbance values at 250, 300, 350, and 500 nm that are representative of UV-C, UV-B, UV-A, and visible spectra, respectively, were used to calculate the T% following eq 5.

$$\text{transmission\%} = 10^{(2-\text{absorbance})} \quad (5)$$

Additionally, a 4 week-long study was performed in simulated tear fluid (STF) to track changes in optical properties of SF films both in dry and wet states.[17] For this purpose, SF films, prepared by different processing conditions, were taken and placed in a 96-well plate. Then, 100 μL of freshly prepared STF was added to each sample and was incubated at 37 °C. Subsequently, at weeks 1, 2, 3, and 4, the absorbance of each sample was recorded at 250, 300, 350, and 500 nm in a multiwell plate reader. The T% was calculated following eq 5, and the data were compared as a function of time.

2.3.6. Degradation Properties. Bioresorbability is a critical parameter for any biomaterial for potential applications in tissue engineering. In the current study, we have analyzed the degradation profile of SF films in a protease solution. Films incubated in STF and PBS were considered for comparison purposes. Briefly, SF films (about 1 × 2 cm long) were immersed in 1 mL of protease XIV (1 U/mL in PBS), STF, or PBS (all three solutions were supplemented with 0.2% w/v sodium azide to prevent any contamination) and the vials were incubated at 37 °C for 24 h. The weight of the films was recorded and this was considered as the initial weight. Subsequently, the films were suspended in fresh fluid and the samples were incubated at 37 °C. The films were collected and weighed at weeks 1, 2, 3, and 4; each time, fresh fluid was replaced. Weight loss % was calculated using eq 6.

$$\text{weight loss (\%)} = \left[\frac{\text{initial weight} - \text{final weight}}{\text{initial weight}}\right] \times 100 \quad (6)$$

https://doi.org/10.1021/acsomega.2c01579
ACS Omega 2022, 7, 29634−29646

2.4. Cell Culture Studies. *2.4.1. Cytotoxicity.* As per ISO 10993, cytotoxicity assay is a mandatory test to be performed for any biomaterial intended for clinical use for any duration and nature of the contact.[18−22] An extract test is performed to determine the cytotoxic effects of a leachable or extract from a material incubated in culture medium or other suitable media. Briefly, on day 1, the test material (SF film) with a surface area of 6 cm^2 was incubated in 1 mL of serum-containing DMEM culture medium at 37 °C and 100 rpm for 24 h. Meanwhile, exponentially proliferating L929 cells at about 1×10^4 cells were seeded per well in a 96-well culture plate and incubated in a CO_2 incubator set at 37 °C for 24 h. Subsequently, on day 2, spent medium from the L929-seeded culture plate was removed, and 100 μL of serum-supplemented culture medium containing with an SF film leachable was added to test wells. The wells fed with culture medium containing dilute phenol (0.13% w/v) and the wells fed with culture medium alone were considered as cytotoxic and noncytotoxic controls, respectively. The culture plate was then incubated back in a CO_2 incubator set at 37 °C for 24 h. Then, on day 3, the cell morphology was photographed, the cells were subjected to MTT assay as per standard protocol, and the metabolic activity (%) was calculated using eq 7.

$$\text{cell viability (\%)} = \frac{\text{absorbance of samples}}{\text{absorbance of cell control}} \times 100 \quad (7)$$

2.4.2. Cytocompatibility with Corneal Cells. Finally, to evaluate the feasibility of SF films for potential applications in corneal tissue engineering, we have performed cell culture studies with the rabbit corneal cell line SIRC. The SIRC cells show mixed fibroblast−epithelial characteristics, yet they were a well-studied cell line for several *in vitro* studies on corneal physiology, drug screening, toxicological testing, and beyond.[23−25] For the cytocompatibility test, SF films prepared from aq, HFIP, and FA approaches were punched into 8 mm circular discs, clipped to cell culture inserts suitable for 24-well plates (Cell Crown, Corning), and sterilized by the ETO (ethylene oxide) method. Before use, each film clipped onto the insert was rinsed twice with PBS and then with medium once. They were then presaturated with fresh DMEM with serum overnight in a CO_2 incubator. Subsequently, the SIRC cell suspension containing about 10,000 cells was seeded onto the top chamber of the inserts and was cultured for 7 days. The same number of cells seeded on 24-well cell culture plates was considered as a control. The cell viability on day 7 was determined by Alamar blue assay as per manufacturer's protocol using eq 8, where O1 is the molar extinction coefficient (E) of oxidized Alamar blue at 570 nm (80,586), O2 is the E of oxidized Alamar blue at 600 nm (117,216), A1 is the absorbance of test wells at 570 nm, A2 is the absorbance of test wells at 600 nm, P1 is the absorbance of cell control at 570 nm, and P2 is the absorbance of cell control at 600 nm.

$$\text{reduction of Alamar blue reagent} = \frac{(O2 \times A1) - (O1 \times A2)}{(O2 \times P1) - (O1 \times P2)} \times 100 \quad (8)$$

Further, to get insights into the qualitative aspects of cell response toward SF films, a cell adhesion study followed by staining for the cytoskeleton and nucleus was performed. For this purpose, SF films were clipped to the inserts, ETO-sterilized, and presaturated as detailed in the previous section. Then, SIRC cells (1×10^4 cells) were seeded and cultured on the test material for 24 h in a CO_2 incubator. Cells cultured on a standard multiwell plate were considered as a control. Subsequently, the cell-laden test material, as well as the control dish, was subjected to staining and imaging. Briefly, samples were washed with 1× PBS for three times, fixed in 4% paraformaldehyde for 1 h at room temperature, washed with PBS for three times, treated with 0.1% Triton X-100 for 3 min, and washed with PBS for three times. Cells were stained with rhodamine-phalloidin (1:100) for 15 min, washed with PBS, counterstained with Hoechst (0.005% w/v in PBS) for 1 min, washed with PBS, and imaged in a fluorescence microscope (Leica DMI 6000B). Subsequently, the cell adhesion was also examined by SEM analysis. For this purpose, cell-laden films were fixed using 4% paraformaldehyde for 1 h. Then, the samples were washed with PBS for 5 min and dehydrated twice using 30, 50, 70, 90, and 100% alcohol for 5 min each. The samples were then treated with isoamyl acetate, followed by critical point drying and gold coating before SEM analysis.

2.5. Statistical Analysis. Typically, at least four replicates for each value were averaged and represented as mean ± SD. Statistical differences were analyzed by either Student's t-test or ANOVA as necessary. Differences were considered significant at a p-value <0.05 and denoted using an asterisk (*) mark. Qualitative images were representative of the respective group.

3. RESULTS

3.1. Morpho-Topographical Properties. The thickness of the films on an average was ranging between 50 and 70 μm. The morphological properties of SF films were analyzed by SEM. As presented in Figure 1, aq films showed relatively rougher surfaces with particulate matter, FA showed rough surfaces with pits, and HFIP films showed smooth surfaces

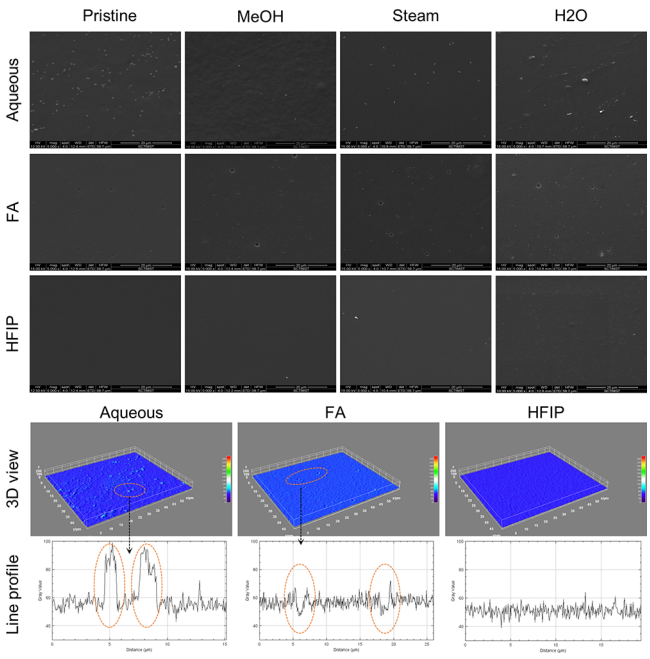

Figure 1. Morphological analysis of silk fibroin films. SEM images of aq, FA, and HFIP films without and with annealing conditions. Representative 3D view and line profiles of aq, FA, and HFIP pristine films are obtained through ImageJ processing. Particulate matter can be seen in the aq film, pits can be seen in the FA film, and the HFIP film was relatively without any artifacts.

https://doi.org/10.1021/acsomega.2c01579
ACS Omega 2022, 7, 29634−29646

without any detectable artifacts. However, it was difficult to detect changes in the surface morphology of the films after the annealing process in all the samples. Further insights into topographical features of SF films were obtained by surface profilometry, which provides roughness values in quantitative terms. As presented in Figure 2, the root mean square

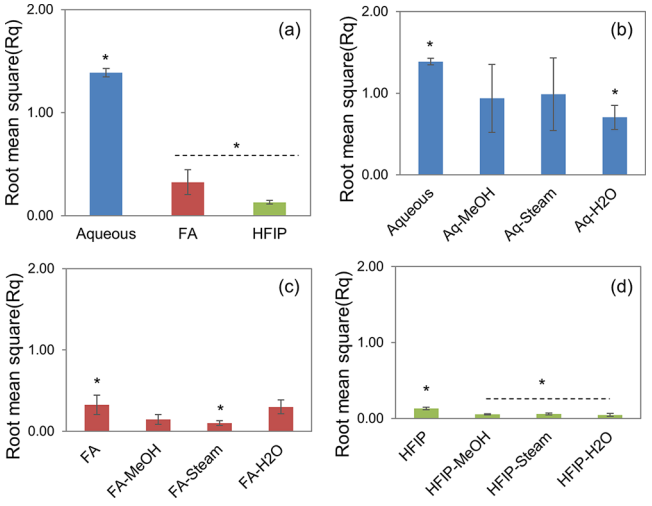

Figure 2. Surface roughness of silk fibroin films. Average surface roughness (Rq) of SF films without and with the postfabrication annealing process (a: aq, FA, and HFIP films without treatment; b: aq films; c: FA films; d: HFIP films) (n = 4; differences between asterisk (*)-marked groups were statistically significant with $p \leq 0.05$).

roughness factor (Rq) values for aq, FA, and HFIP solvents were found to be 1.39, 0.32, and 0.13, respectively. These data confirmed the gross scale roughness profile observed in SEM showing greater roughness in the aq solvent, followed by FA and HFIP solvents. Concerning the effect of annealing on roughness factor, aq, FA, and HFIP films showed nearly 50% reduction in roughness factor after the annealing process in general. For instance, the Rq of aq films reduced from 1.39 to 0.70, the Rq of FA films reduced from 0.32 to 0.10, and the Rq of FA films reduced from 0.13 to 0.06. Therefore, the topography was affected by, or in other words, can be modulated by, fabrication as well as postfabrication process parameters.

3.2. Physical Properties. Surface wettability is a critical parameter to be determined for any biomaterial intended for use in tissue engineering applications. Typically, this gives an idea about the hydrophilicity/hydrophobicity of the material and therefore defines the cell−material interactions. Usually, this is measured by determining the surface contact angle. In the current study, the sessile drop technique in a computer-controlled goniometer was followed to determine the effect of process parameters on the contact angle of SF films. As presented in Table 1, aq, FA, and HFIP films showed contact angles of about 73°, 85°, and 89°, respectively. All the films were hydrophilic; however, the contact angle increased in the order of aq < FA ≈ HFIP. Upon postfabrication annealing, the contact angle was slightly enhanced in aq films, whereas in FA and HFIP films, it was slightly reduced.

Besides surface wettability, it is also important to analyze the bulk wettability, i.e., the water uptake capacity of a biomaterial. It is equally important to evaluate the swelling property of the biomaterial. In the current study, we have determined water uptake % and swelling ratio by determining the amount of water absorbed and the weight gained using eqs 1 and 2, respectively. As shown in Table 2, aq, FA, and HFIP films exhibited water uptake % values of about 58, 29, and 27%, respectively. Upon postfabrication annealing, the water uptake % was reduced among all the samples, wherein steam-annealed samples showed the lowest water uptake % values. Similarly, as presented in Table 3, the swelling ratio was 1.58 in aq films and it was reduced to 1.3 in FA films and 1.28 in HFIP films. Also, upon annealing, the swelling ratio was reduced, wherein steam-annealed samples showed the lowest swelling ratio.

Another parameter to consider is the water vapor transmission (WVT), which is calculated to understand the transmission of water vapors through a biomaterial, typically in the form of films. In the current study, we determined WVT % by calculating the loss of water kept in a vial having a lid fitted with SF films. The weight loss of the vials was determined over a specific time point, and the values were fit into eqs 3 and 4. A vial without any lid was considered as a control. The results are presented in Table 4: aq films showed a WVT% of 39%, FA showed 26%, and HFIP showed 22% with respect to the control. Upon annealing, WVT% was reduced in aq films but slightly enhanced in FA and HFIP films. A vial fit with a commercial dialysis membrane was used for comparison purposes, which showed a WVT% of 66%.

3.3. Chemical/Structural Properties. The effect of fabrication and postfabrication processes on SF film composition and secondary structural features was assessed by FTIR spectroscopy. As presented in Figure 3, typically degummed SF fiber exhibits a peak at 1620 cm^{-1}, reflecting the highly ordered β-sheet structure of the protein. Upon aqueous reconstitution, the conformational changes from ordered to unordered elements took place and this was reflected by a peak shift to 1640 cm^{-1}. After fabrication and annealing, all the films showed a peak shift back to 1620 cm^{-1}, which was an indication of conformational change from a less ordered structure to a highly ordered structure typically dominated by β-sheet elements. Further, the analysis of the full spectrum of all the samples showed a consistent spectral pattern among the films, i.e., no new peaks were found or no deletion of characteristic peaks was observed, and thus indicated an unaltered composition across various fabrication and annealing processes.

3.4. Mechanical Properties. Native corneal tissue is a mechanically tough biological material with Young's modulus ranging between 0.1 and 57 MPa with notable differences

Table 1. Effect of Process Parameters on the Contact Angle of SF Films[a]

	pristine	MeOH	steam	H_2O
aqueous	72.9 ± 0.8*	76.55 ± 2.7	88.7 ± 2.6*	73.8 ± 1.4
FA	85.05 ± 1.7*	83.4 ± 1.8	75.5 ± 2.4*	74.7 ± 1.5*
HFIP	88.9 ± 9.3	85.9 ± 2.6	84.4 ± 2.2	83.9 ± 1.6

[a] n = 4; differences between asterisk (*)-marked groups were statistically significant with $p \leq 0.05$.

https://doi.org/10.1021/acsomega.2c01579
ACS Omega 2022, 7, 29634−29646

Table 2. Effect of Process Parameters on the Water Uptake % of SF Films[a]

	pristine	MeOH	steam	H_2O
aqueous	57.6 ± 4.7*	51.8 ± 1.1*	23.3 ± 0.3*	42.8 ± 3.2*
FA	29.5 ± 1.7*	28.3 ± 4.8	14.2 ± 1.8*	22.6 ± 1.1*
HFIP	27.3 ± 0.1*	24.7 ± 0.3*	16 ± 2.9*	23 ± 2.9*

[a] $n = 4$; differences between asterisk (*)-marked groups were statistically significant with $p \leq 0.05$.

Table 3. Effect of Process Parameters on the Swelling Ratio of SF Films[a]

	pristine	MeOH	steam	H_2O
aqueous	1.58 ± 0.05*	1.52 ± 0.01	1.23*	1.43 ± 0.03
FA	1.3 ± 0.02*	1.28 ± 0.05	1.14 ± 0.02*	1.23 ± 0.01*
HFIP	1.28 ± 0.09*	1.25	1.16 ± 0.03*	1.22 ± 0.1

[a] $n = 4$; differences between asterisk (*)-marked groups were statistically significant with $p \leq 0.05$.

Table 4. Effect of Process Parameters on the WVT% of SF Films[a]

	pristine	MeOH	steam	H_2O
aqueous	39.15%*	34.60%	29.65%*	33.61%
FA	25.57%	27.10%	33.28%	30.65%
HFIP	22.58%	26.16%	24.63%	27.10%

[a] Closed system: 0.30%; open system: 100% ($n = 4$; differences between asterisk (*)-marked groups were statistically significant with $p \leq 0.05$).

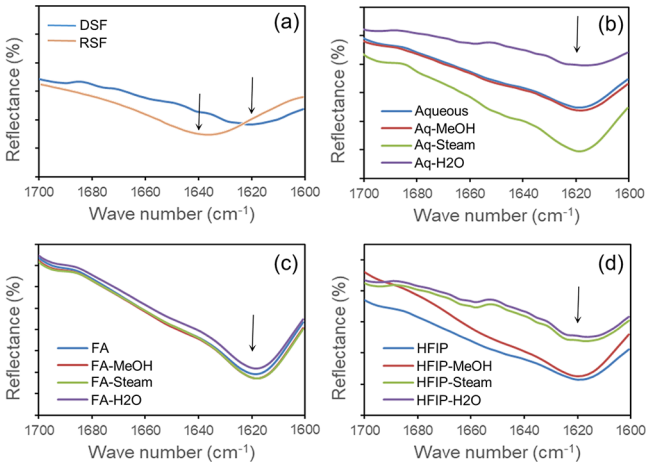

Figure 3. ATR-FTIR spectral data of silk fibroin films. (a) DSF and RSF (degummed and reconstituted SF), (b) aq films, (c) FA films, and (d) HFIP films indicated the compositional/structural elements across prefabrication, fabrication, and postfabrication annealing processes.

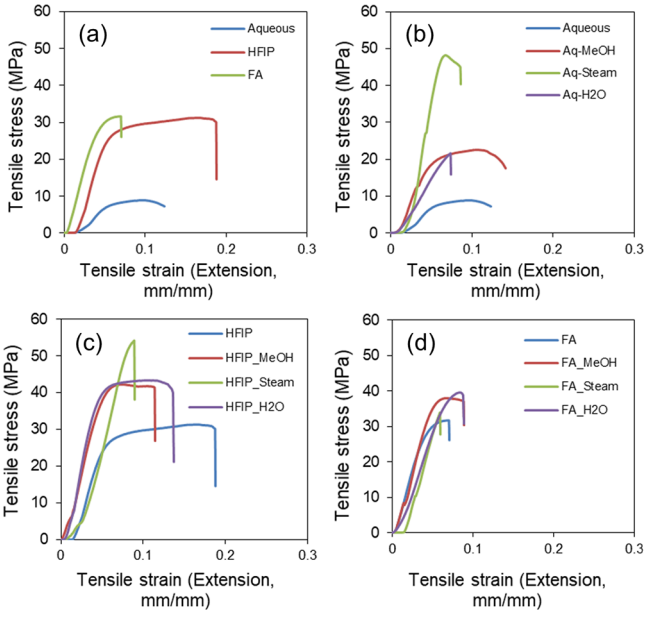

Figure 4. Tensile testing data of silk fibroin films. (a) aq, HFIP, and FA films without annealing, (b) aq films with annealing, (c) HFIP films with annealing, and (d) FA films with annealing indicated the changes in tensile strength with respect to process parameters.

based on the stromal region characterized, age of the donor, storage period, and measurement technique followed. In the current study, the effect of process parameters on the mechanical properties of SF films was determined by tensile testing. First, the SF films prepared by aq, HFIP, and FA solvents were compared, and as can be seen from Figure 4a, the aq film showed relatively low tensile strength followed by the HFIP film, and the FA film showed relatively high tensile strength. Subsequently, aq, HA, and FA films with the postfabrication annealing process, viz. H_2O, MeOH, and steam, were tested. Figure 4b,c indicated that, for both aq and HFIP cases, the tensile property was enhanced after the annealing process, wherein H_2O- and MeOH-annealed films showed a nearly comparable profile, whereas steam-annealed films showed the highest tensile strength. As presented in Figure 4d, FA films showed comparable tensile property profiles with or without annealing, indicating no significant postfabrication effect.

3.5. Degradation Properties. Bioresorbability is a critical parameter for any biomaterial for potential applications in tissue engineering. In the current study, we have analyzed the degradation profile of SF films in three different media over 4 weeks at 37 °C. To compare the effect of fabrication processing, aq, FA, and HFIP films without annealing were used, and to compare the effect of postfabrication processing, HFIP films annealed with water vapor, methanol vapor, and steam were used. The weight loss % is determined and presented in Figure 5. Gradual weight loss was noticed in all the films irrespective of the medium. However, at week 4, aq films showed significantly higher degradation in enzyme solution with a weight loss of about 72%, followed by HFIP films with a weight loss of about 41% and then FA films with only about 12% weight loss. Among annealed samples, HFIP-H_2O films showed 29% weight loss, HFIP-MeOH films showed 21% weight loss, and HFIP-steam films showed 15%

https://doi.org/10.1021/acsomega.2c01579
ACS Omega 2022, 7, 29634−29646

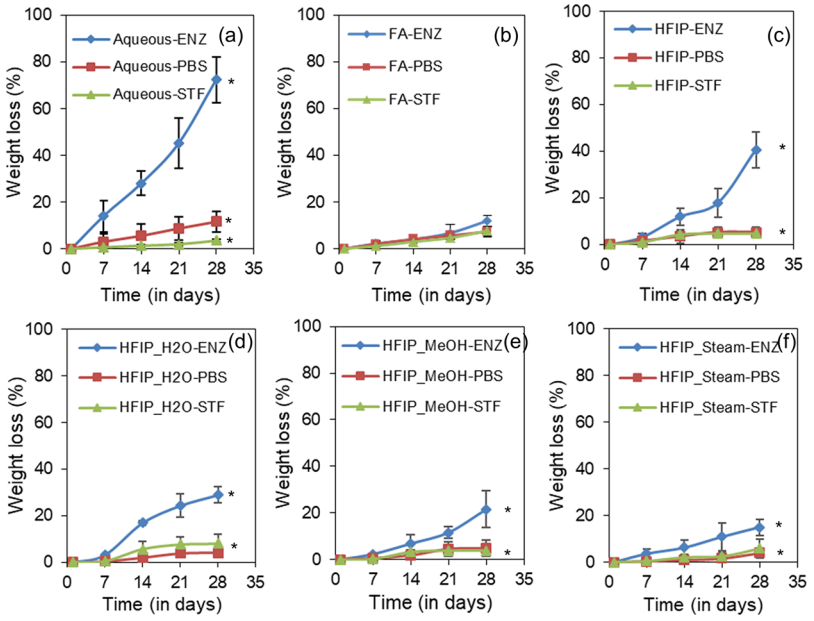

Figure 5. Biodegradation profile of silk fibroin films. Weight loss % values of SF films in a protease (ENZ), phosphate-buffered saline (PBS), and simulated tear fluid (STF) over 4 weeks of incubation (a: aq plots; b: FA plots; c: HFIP plots (all without annealing); d: HFIP-water-annealed plots; e: HFIP-methanol-annealed plots; f: HFIP-steam-annealed plots) (n = 4; differences between asterisk (*)-marked groups were statistically significant with $p \leq 0.05$).

weight loss at week 4. Annealed films in PBS and STF showed negligible degradation.

3.6. Optical Properties. Optical clarity is the foremost criterion for consideration while designing a biomaterial for corneal tissue engineering applications. Therefore, in this current study, we have focused on the optical properties and investigated if there were any process (fabrication and postfabrication)-dependent variations. As presented in Figure 6, SF films from all three solvents such as aq, FA, and HFIP solvents, with and without annealing, showed excellent optical clarity. Typically, in the native state, the cornea was covered with a tear film and therefore remains in a wet state at all times. To this end, we have incubated SF films in water and recorded the changes in optical clarity after wetting. As can be seen from the figure, SF films showed remarkable optical clarity even in a wet state, irrespective of processing conditions.

To get further insights into optical properties, we analyzed the absorption spectra of SF films by UV−Vis spectroscopy from 200 to 700 nm wavelength in a multiwell plate reader. As presented in Figure 7, the results indicated that all SF films in the dry state showed almost negligible absorbance in the visible region (500 nm), irrespective of the fabrication and annealing process. Subsequently, to simulate the wet state condition of the cornea as in natural condition, we have wetted the SF films and recorded the spectra once again and found no notable changes in the absorbance of the sample before and after wetting. Similarly, negligible absorbance was recorded at UVA (350 nm) and UVC (250 nm) regions in all the films, both in the dry and wet states, but relatively high absorbance was recorded at the UVB (300 nm) region, perhaps indicating the typical absorption shown by proteins at 280 nm.

Further, to get quantitative information on the optical properties of SF films, we have taken the spectra at representative wavelengths and calculated T%. As presented in Figure 8a, similar to previous observations, all SF films in the dry state showed almost 90% transmission in the visible region

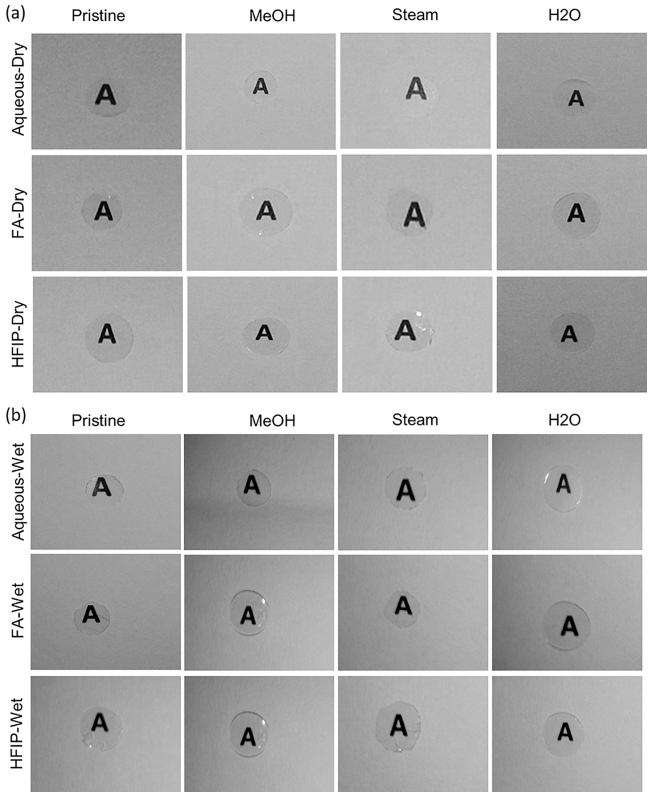

Figure 6. Optical clarity of silk fibroin films. aq, FA, and HFIP solvent-derived SF films without annealing and with annealing with methanol, steam, and water showed excellent optical clarity in (a) a dry state as well as in (b) a wet state.

(500 nm) across various fabrication and annealing processes. We have calculated T% for wet samples and found no significant changes between dry and wet samples. To check if the long-term wetting influences the optical clarity of SF films,

https://doi.org/10.1021/acsomega.2c01579
ACS Omega 2022, 7, 29634−29646

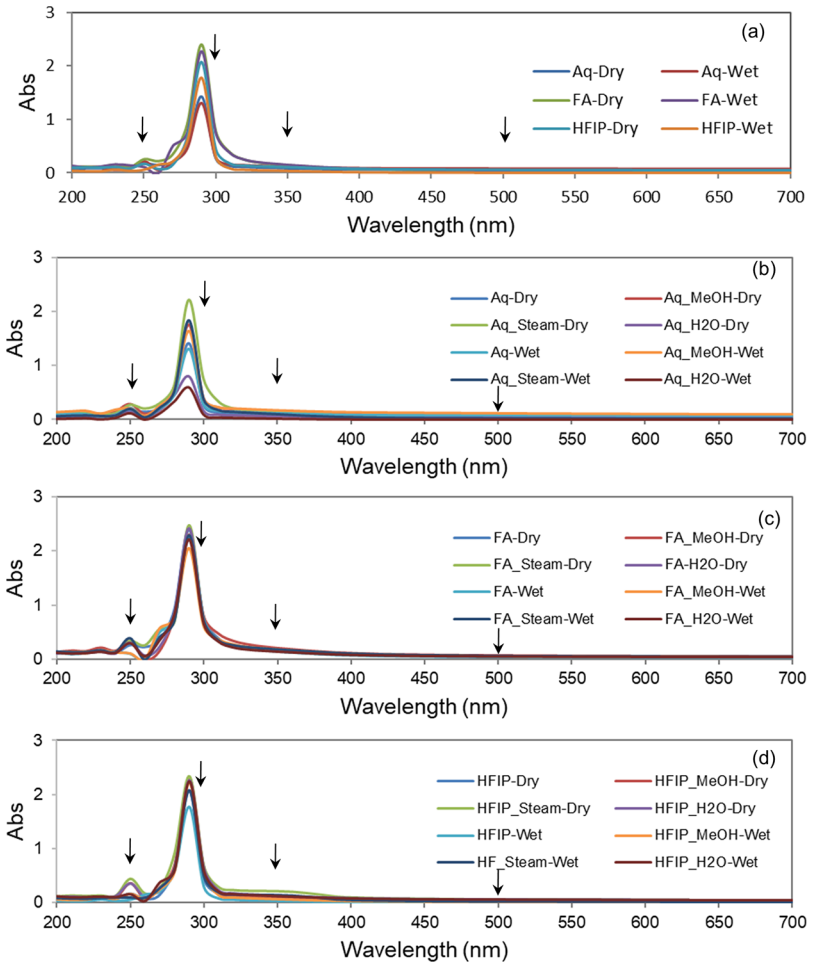

Figure 7. UV−Vis spectral data of silk fibroin films. Absorption spectra of (a) aq, FA, and HFIP films without annealing, (b) aq films with and without annealing, (c) FA films with and without annealing, and (d) HFIP films with and without annealing (arrows indicate representative UVC, UVB, UVA, and visible spectral regions at 250, 300, 350, and 500 nm, respectively).

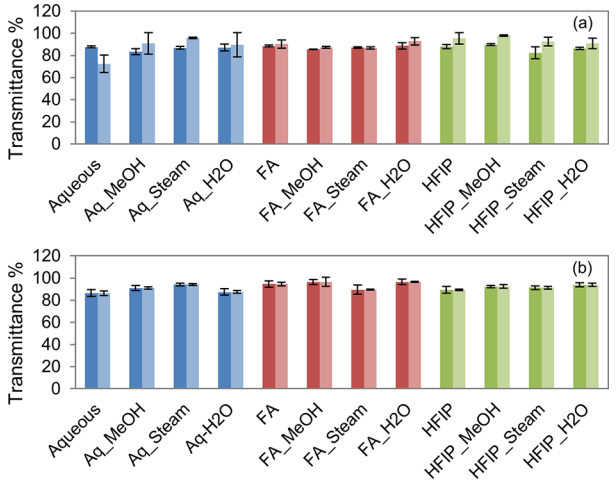

Figure 8. Transmittance % of silk films. The *T*% of aq, FA, and HFIP films with and without annealing at the visible range on day 1 (a, dark bars represent the dry state and light bars represent the wet state) and day 28 (b, dark bars show week 1 data and light bars show week 4 data) indicated that there were no significant changes on the optical clarity of SF films even after wetting in STF for 4 weeks.

the films were incubated in STF for 4 weeks, the absorbance was recorded, and *T*% was calculated. As presented in Figure 8b, all the films (with and without annealing) showed about 90% transmission and there was no significant difference in *T*% even after 4 weeks of incubation in STF.

3.7. Cytotoxicity. The cytotoxicity of the SF films prepared by different processing conditions was investigated following an extract assay test and MTT assay as per ISO 10993-5. The extract assay test is a well-known cytotoxicity assay that involves the microscopic examination of changes in cell morphology in response to test and control samples. As can be seen in Figure 9, cells treated with the test sample extracts (aq, FA, and HFIP solvents with and without annealing) showed good morphology similar to that of cell control; therefore, they were considered as noncytotoxic (grade 0), whereas the cells treated with phenol showed severe cytotoxicity (grade 4) as anticipated. Meanwhile, MTT assay was used for obtaining the quantitative measurement of the cell viability. In the current study, about 80−100% cell viability was observed in the test samples. As per ISO 10993-5, a reduction in cell viability by >30% is considered a cytotoxic effect; since all the test samples showed reduction by <30%, they were considered noncytotoxic.

3.8. Cytocompatibility with Corneal Cells. Finally, we have investigated the ability of the SF films, prepared by different processing conditions, to support corneal cells for subsequent application in corneal tissue engineering. For this purpose, we have cultured SIRC cells (rabbit corneal cells) on

https://doi.org/10.1021/acsomega.2c01579
ACS Omega 2022, 7, 29634−29646

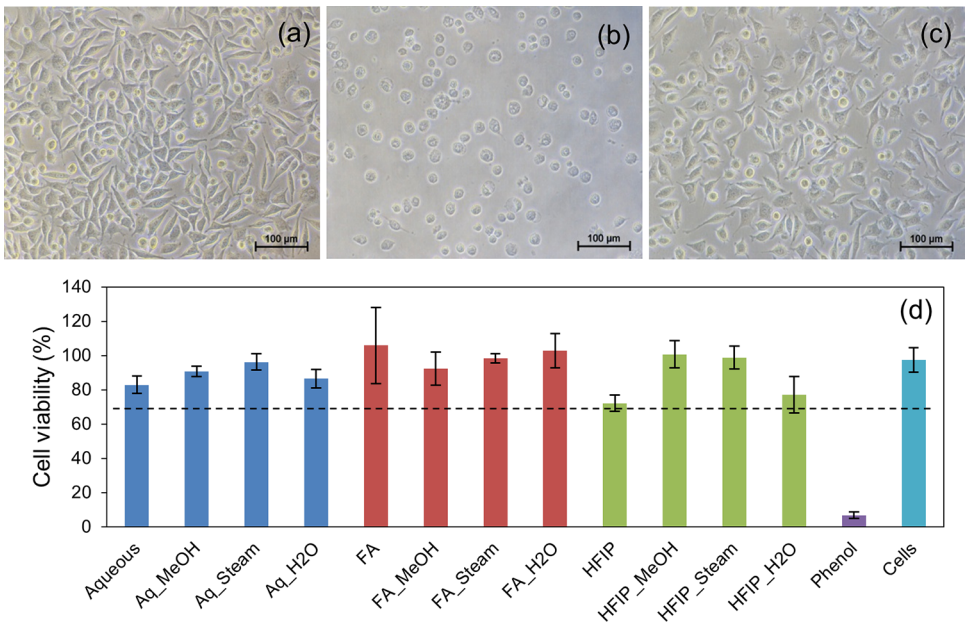

Figure 9. Cytotoxicity profile of SF films. Inverted phase contrast image of cells treated with extracts of the test sample (a), phenol (b), and cell control (c); percentage viability of cells as measured by MTT assay (d). All the test samples showed >70% cell viability and thus were considered noncytotoxic.

SF films and determined cell viability and cell adhesion with respect to cells cultured on TCPS (tissue culture polystyrene dish). As presented in Figure 10, aq, HA, and FA films without annealing and aq films with MeOH, H_2O, and steam annealing showed comparable cell viability, with 70−80% cell viability with respect to cells cultured on TCPS. Cell viability on TCPS vs that on test samples was statistically significant, perhaps due to the fact that TCPS was tissue culture-treated, whereas the test samples were without any coating. Subsequently, cell-laden test samples were stained with cytoskeletal and nuclear stains to check cell adhesion patterns. As presented in Figure 11, a good number of cells were found to adhere and well spread with typical corneal epithelial morphology (ovoid to cuboidal) on the test samples, similar to the TCPS control. The SEM analysis of cell-laden films, as shown in Figure 12, confirmed that SIRC cells were nicely adhered and spread on the SF films similar to those on TCPS. Further, as mentioned in earlier sections, optical clarity is the critical characteristic property of a biomaterial for corneal tissue engineering. To confirm the transparency after cell culture studies, the cell-laden test materials were visually observed and photographed. As presented in Figure 13, all the test samples under study were found to be clear and optically transparent. Overall, the SF films prepared by different processing conditions were found to be equally compatible with corneal cells for potential application in corneal tissue engineering.

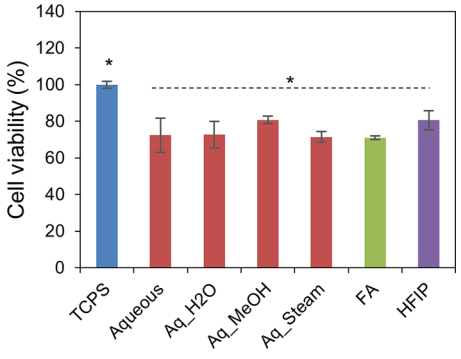

Figure 10. Cell viability % of SIRC cells on SF films. aq, HFIP, and FA films without annealing and aq films with MeOH, H_2O, and steam annealing showed comparable cell viability, with 70−80% cell viability with respect to cells cultured on TCPS (n = 6; differences between asterisk (*)-marked groups were statistically significant with $p \leq 0.05$).

4. DISCUSSION

Cornea, a transparent, protective, outermost layer of the eye, provides 75% of total refractive power and transmits 98% red light and 90% blue light. The lack of donors, the possibility of infections, and rejection rates made researchers find an alternative therapy method. To this end, tissue engineering has emerged as an alternative therapeutic approach that involves the creation of bioartificial tissues *in vitro* by culturing cells of patients or healthy donors on a biomaterial scaffold in the presence of bioactive growth factors.[26] Unlike other natural polymers, the amenability of silk to be processed into a wide array of formats suiting for different applications serves an extra credit. Robust mechanical properties, tunable degradation patterns, and chemical properties aid its usage in different fields. Due to the presence of additional desirable characteristics, SF and blends of SF have gained the attention of scientists all over the world. Although a huge number of studies have been performed with SF in tissue engineering, no study was taken up so far to investigate process-dependent variations in SF films, particularly in the context of corneal tissue engineering. The current study was aimed to fill the gap and provide insights into fabrication- and postfabrication-dependent variations in silk films. A bird's eye view of the overall observations is presented in Figure 14.

Morpho-topological analysis by SEM and surface profilometry revealed a decrease in roughness in the order of aq (Rq = 1.39) > FA (Rq = 0.32) > HFIP (Rq = 0.13). This was

https://doi.org/10.1021/acsomega.2c01579
ACS Omega 2022, 7, 29634−29646

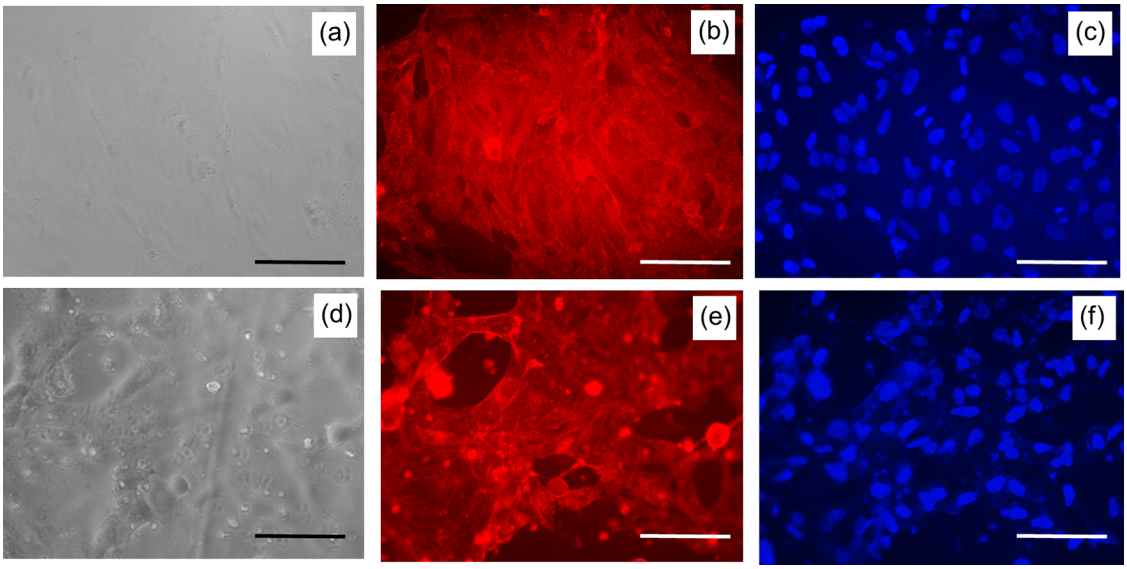

Figure 11. Cell adhesion on SF films. SIRC cells adhered and spread well on SF films similar to that on TCPS control (a−c: TCPS; d−f: aq SF films; a, d: phase contrast: b, e: cytoskeleton stained with rhodamine-phalloidin; c, f: nuclei stained with Hoechst).

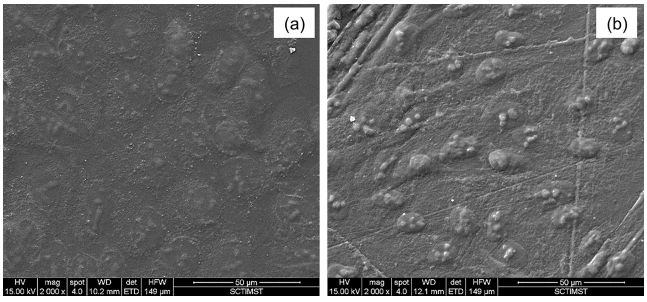

Figure 12. Cell adhesion study. SEM images of SIRC cells on TCPS (a) and aq SF films (b) showed well adhered and nicely spread morphology.

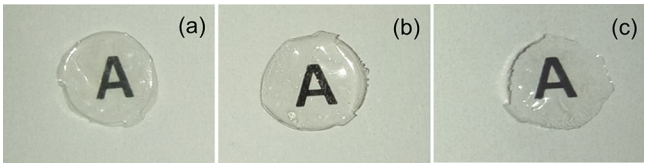

Figure 13. Transparency of SF films after cell adhesion studies. All the test materials were found to retain their transparency even after cell culture (a: aq; b: FA; c: HFIP).

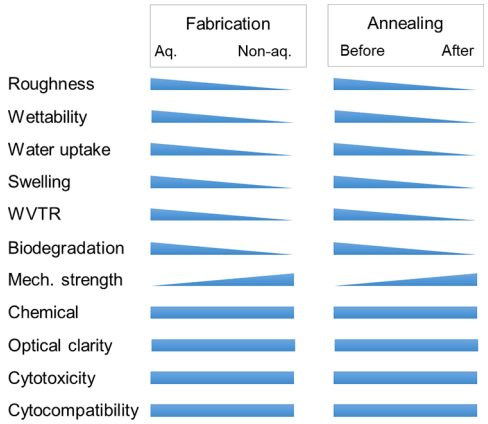

Figure 14. Bird's eye view of the process−property−function relationship in silk film fibroins films. The graphic depicts the influence of fabrication (aqueous vs non-aqueous) and postfabrication (pristine vs annealed) processes on various properties of silk films. Note that the relationship shown is representative in nature and not to any scale.

reduced by nearly 50% after the annealing process in general. Recently, Yang et al. reported the surface morphology of *B. mori*/tussah SF blend films, wherein they observed smoother surface morphology in FA films than aq films.[27] Thus, the process-dependent variations in morpho-topological properties of SF films in our study were comparable with earlier reports. On the other hand, Zhang et al. and Luangbudnark et al. evaluated wettability, water uptake, swelling, and WVT% and found that the films were hydrophilic; meanwhile, the swelling ratio of the films was in the range of 48−57%.[16,28] They also evaluated SF films conjugated with curcumin for WVT% and found them to have better permeability as that of our results. In the current study, when compared to the films made from the aq solvent, the films made from FA or HFIP solvents were showing reduced interaction with water in general. Further, upon annealing, compared to H_2O- and MeOH-annealed films, the steam-annealed films showed reduced interaction with water, as reflected in the contact angle, water uptake, swelling ratio, and WVT%. Therefore, the effects of process conditions on the physical properties of SF films were evident and were in good agreement with earlier reports.

Kasoju et al. and Jaramillo-Quiceno et al. evaluated the FTIR spectra of SF and reported that SF was characterized by amide I, II, and III bands.[12,29] In particular, the amide I band position was explored to get details of the secondary structure of SF, where degummed SF fiber typically showed a silk II structure, which changes to silk I upon aqueous reconstitution and then reverses back to silk II upon processing into films and sponges, which can be relatable to our results. As for tensile properties, the relative strength was found to increase in the order of aq < HFIP < FA for control films. The tensile strength was enhanced in both aq and HFIP films after the annealing process. Previously, Rajkhowa et al. reported that aq films

https://doi.org/10.1021/acsomega.2c01579
ACS Omega 2022, 7, 29634−29646

showed a tensile strength of 3.5 MPa, which was increased to 15.8 MPa after ethanol annealing; also, FA films annealed with ethanol showed a relatively high tensile strength of 43.6 MPa.[30] These observations correlate well with our experimental results. One interesting observation noted in our study was that, in the case of FA, the tensile properties seem to be comparable among non-annealed and annealed samples. Perhaps, this could be due to the widely accepted notion that FA induces β-sheet formation to the maximum extent possible with no further scope for molecular arrangement, as evident from the nearly identical FITR spectral pattern.

As for biodegradation properties, previously, Rajkhowa et al. reported that aq films showed 62% weight loss, whereas FA films showed only 2.8% in an aqueous medium.[30] In the current study, upon enzymatic degradation, aq films lost by 72%, HFIP films lost by 41%, and FA films lost by 12%. Among annealed samples, HFIP-H_2O lost by 29%, HFIP-MeOH lost by 21%, and HFIP-steam lost by 15%. There was a clear effect of fabrication and postfabrication processing conditions on the biodegradation properties of SF films, in good agreement with earlier reports. Once again, the resistance of FA films for degradation may be due to the secondary structural elements in SF. Yao et al., Ha et al., and Liu et al. reported that FA was an attractive solvent for inducing the conformational changes toward the β-sheet structure in SF and thereby modulating the unique properties of SF materials.[31−33] Although HFIP was found to induce the silk II structure in SF, in the current study, it appeared that the silk II component was relatively less in HFIP films than in FA films. This has to be looked at in detail, probably by analyzing the secondary structure details by CD spectroscopy or other similar techniques.

Optical property is the most critical feature for consideration when developing biomaterials for ophthalmic applications. In the current study, the SF films showed about 90% *T*% in the visible range, irrespective of fabrication and postfabrication processing conditions followed. There were no notable differences in optical properties of SF films in dry and wet states. Further, a 4 week-long incubation study also confirmed that the SF films remained to be optically clear. Qi et al. reported the preparation of SF-based flexible and conductive films and showed that the films possessed 80−90% *T*% even after blending with other components.[34] Also reported was the preparation of SF films with a focus on assessing the effects of degumming process parameters on film properties, where they found excellent transparency in all the films; however, the transparency tends to change after wetting the films. Liu et al. also evaluated and reported about 90% *T*% of SF films in the visible light spectrum. Collectively, these reports fall in line with our observations on SF film optical properties.[35]

With respect to the cytotoxicity of SF films, previously, Akturk et al. reported about 90% cell viability of L929 cells treated with extracts of SF/gold nanoparticle 3D matrices as per ISO 10993-5, similar to our results.[36] Next, we have investigated the cytocompatibility of SF films for corneal tissue engineering applications using SIRC cells (rabbit corneal cells). Alamar blue assay indicated 70−80% cell viability in all the test samples, and subsequent cytoskeletal staining and SEM analysis of cell-laden test samples showed a good number of well-adhered and well-spread cells with typical corneal epithelial morphology (ovoid to cuboidal). Our results match with earlier reports such as those of Hazra et al., Liu et al., and a few others who have reported the compatibility of SF-based biomaterials with corneal cells for corneal tissue engineering applications.[37,38] Further, we also showed in this study that the transparency remains unaltered even after cell culture studies. Our results match with those of Kim et al. who reported that *Aloe vera* gel blended SF films showed excellent cornea endothelial cell regeneration without any effect on optical clarity.[39]

5. CONCLUSIONS

With a hypothesis that various fabrication and postfabrication processing conditions could influence the properties and function of SF films in the context of corneal tissue engineering, we have prepared SF films by using three different solvents (aq, FA, and HFIP), with postfabrication processing in three different conditions (methanol vapor, water vapor, and steam), and subsequently investigated their various properties. The results concluded that the fabrication and postfabrication conditions indeed affect the topological, physical, tensile, and degradation properties of SF films to a significant extent; however, the effects on chemical composition, optical properties, and cytocompatibility were negligible. That means that SF films were prone to processing changes in various physicochemical properties, yet they remain optically clear, noncytotoxic, and cytocompatible with corneal cells. This opens an avenue for choosing an appropriate processing method for preparing SF films with a set of physical/tensile/degradation properties of choice without compromising optical clarity and cytocompatibility. However, the effect of these process parameters on the molecular fingerprint of corneal epithelial cells, the ability to stratify during air−liquid interface culture, and *in vivo* performance in animal models is yet to be explored.

AUTHOR INFORMATION

Corresponding Author

Naresh Kasoju − *Division of Tissue Culture, Department of Applied Biology, Biomedical Technology Wing, Sree Chitra Tirunal Institute for Medical Science and Technology, Thiruvananthapuram 695012 Kerala, India;* orcid.org/0000-0002-8700-0729; Email: naresh.kasoju@sctimst.ac.in

Authors

Maya Beena − *Division of Tissue Culture, Department of Applied Biology, Biomedical Technology Wing, Sree Chitra Tirunal Institute for Medical Science and Technology, Thiruvananthapuram 695012 Kerala, India;* orcid.org/0000-0001-6546-8278

Jimna Mohamed Ameer − *Division of Tissue Culture, Department of Applied Biology, Biomedical Technology Wing, Sree Chitra Tirunal Institute for Medical Science and Technology, Thiruvananthapuram 695012 Kerala, India*

Complete contact information is available at: https://pubs.acs.org/10.1021/acsomega.2c01579

Author Contributions

M.B. provided the methodology, curated the data, and carried out the formal analysis and writing of the original draft of the manuscript. J.M.A. provided the methodology. N.K. conceptualized the study, curated the data, and performed the formal analysis, funding acquisition, project administration, supervision, and review and editing of the manuscript.

https://doi.org/10.1021/acsomega.2c01579
ACS Omega 2022, 7, 29634−29646

Notes

The authors declare no competing financial interest.

■ ACKNOWLEDGMENTS

The authors thank the Director and the Head of Biomedical Technology Wing, Sree Chitra Tirunal Institute for Medical Sciences and Technology, Thiruvananthapuram, for providing financial support through Technology Development Fund (P6219) to the PI and for the MPhil fellowship to M.B.. The authors thank Mrs. Nimi N. for contact angle measurements, Mrs. Sasikala T. C. for FTIR readings, Mr. Chandra Shekhar Nayak for tensile testing, Mr. Nishad K. V. for SEM analysis, Mr. Jithu Raj for surface profilometry analysis, and Ms. Anju M. S. and Ms. Athira R. K. for cell culture studies. The authors extend their thanks to Dr. Prabha D. Nair, Dr. Renjith S, Dr. Roy Joseph, Dr. Manoj Komath, Dr. Anil Kumar P. R., and Er. Leena Joseph, Scientist in Charge of various divisions, for offering the facilities.

■ REFERENCES

(1) Peh, G. S. L.; Beuerman, R. W.; Colman, A.; Tan, D. T.; Mehta, J. S. Human Corneal Endothelial Cell Expansion for Corneal Endothelium Transplantation: An Overview. *Transplantation* **2011**, *91*, 811−819.

(2) Kasoju, N.; Bora, U. Silk Fibroin in Tissue Engineering. *Adv. Healthcare Mater.* **2012**, *1*, 393−412.

(3) Dicko, C.; Kasoju, N.; Hawkins, N.; Vollrath, F. Differential Scanning Fluorimetry Illuminates Silk Feedstock Stability and Processability. *Soft Matter* **2016**, *12*, 255−262.

(4) Narita, C.; Okahisa, Y.; Wataoka, I.; Yamada, K. Characterization of Ground Silk Fibroin through Comparison of Nanofibroin and Higher Order Structures. *ACS Omega* **2020**, *5*, 22786−22792.

(5) Zhang, F.; Yang, R.; Zhang, P.; Qin, J.; Fan, Z.; Zuo, B. Water-Rinsed Nonmulberry Silk Film for Potential Tissue Engineering Applications. *ACS Omega* **2019**, *4*, 3114−3121.

(6) Gomes, D. S.; da Costa, A.; Pereira, A. M.; Casal, M.; Machado, R. Biocomposites of Silk-Elastin and Essential Oil from *Mentha Piperita* Display Antibacterial Activity. *ACS Omega* **2022**, *7*, 6568−6578.

(7) Mondal, M.; Trivedy, K.; Irmal Kumar, S. The Silk Proteins, Sericin and Fibroin in Silkworm, Bombyx Mori Linn., A Review. *Casp. J. Environ. Sci* **2007**, *5*, 63−16.

(8) Li, G.; Li, Y.; Chen, G.; He, J.; Han, Y.; Wang, X.; Kaplan, D. L. Silk-Based Biomaterials in Biomedical Textiles and Fiber-Based Implants. *Adv. Healthcare Mater.* **2015**, *4*, 1134−1151.

(9) Mohamed Ameer, J.; Venkatesan, R. B.; Damodaran, V.; Nishad, K. V.; Arumugam, S.; Pallickaveedu Rajan Asarie, A. K.; Kasoju, N. Fabrication of Co-Cultured Tissue Constructs Using a Dual Cell Seeding Compatible Cell Culture Insert with a Clip-on Scaffold for Potential Regenerative Medicine and Toxicological Screening Applications. *J. Sci.: Adv. Mater. Devices* **2020**, *5*, 207−217.

(10) Mukherjee, S.; Krishnan, A.; Athira, R. K.; Kasoju, N.; Sah, M. K. Silk Fibroin and Silk Sericin in Skin Tissue Engineering and Wound Healing: Retrospect and Prospects. In *Natural Polymers in Wound Healing and Repair*; Elsevier, 2022; pp. 301−331, DOI: 10.1016/B978-0-323-90514-5.00005-5.

(11) Tamada, Y. New Process to Form a Silk Fibroin Porous 3-D Structure. *Biomacromolecules* **2005**, *6*, 3100−3106.

(12) Kasoju, N.; Hawkins, N.; Pop-Georgievski, O.; Kubies, D.; Vollrath, F. Silk Fibroin Gelation via Non-Solvent Induced Phase Separation. *Biomater. Sci.* **2016**, *4*, 460−473.

(13) Bray, L. J.; George, K. A.; Ainscough, S. L.; Hutmacher, D. W.; Chirila, T. V.; Harkin, D. G. Human Corneal Epithelial Equivalents Constructed on Bombyx Mori Silk Fibroin Membranes. *Biomaterials* **2011**, *32*, 5086−5091.

(14) Lu, Q.; Hu, X.; Wang, X.; Kluge, J. A.; Lu, S.; Cebe, P.; Kaplan, D. L. Water-Insoluble Silk Films with Silk I Structure. *Acta Biomater.* **2010**, *6*, 1380−1387.

(15) Rockwood, D. N.; Preda, R. C.; Yücel, T.; Wang, X.; Lovett, M. L.; Kaplan, D. L. Materials Fabrication from Bombyx Mori Silk Fibroin. *Nat. Protoc.* **2011**, *6*, 1612−1631.

(16) Zhang, X.; Chen, Z.; Bao, H.; Liang, J.; Xu, S.; Cheng, G.; Zhu, Y. Fabrication and Characterization of Silk Fibroin/Curcumin Sustained-Release Film. *Materials* **2019**, *12*, 3340.

(17) Kotreka, U. K.; Davis, V. L.; Adeyeye, M. C. Development of Topical Ophthalmic In Situ Gel-Forming Estradiol Delivery System Intended for the Prevention of Age-Related Cataracts. *PLoS One* **2017**, *12*, No. e0172306.

(18) ISO 10993-1:2018, Biological Evaluation of Medical Devices — Part 1: Evaluation and Testing within a Risk Management Process. International Organization for Standardization.

(19) ISO 10993-5:2009, Biological Evaluation of Medical Devices — Part 5: Tests for in Vitro Cytotoxicity. International Organization for Standardization.

(20) ISO 10993-12:2021, Biological Evaluation of Medical Devices — Part 12: Sample Preparation and Reference Materials. International Organization for Standardization.

(21) Baek, H. S.; Yoo, J. Y.; Rah, D. K.; Han, D.-W.; Lee, D. H.; Kwon, O.-H.; Park, J.-C. Evaluation of the Extraction Method for the Cytotoxicity Testing of Latex Gloves. *Yonsei Med. J.* **2005**, *46*, 579.

(22) Srivastava, G. K.; Alonso-Alonso, M. L.; Fernandez-Bueno, I.; Garcia-Gutierrez, M. T.; Rull, F.; Medina, J.; Coco, R. M.; Pastor, J. C. Comparison between Direct Contact and Extract Exposure Methods for PFO Cytotoxicity Evaluation. *Sci. Rep.* **2018**, *8*, 1425.

(23) Iwatsuka, K.; Iwamoto, H.; Kinoshita, M.; Inada, K.; Yasueda, S.; Kakehi, K. Comparative Studies of *N* -Glycans and Glycosaminoglycans Present in SIRC (Statens Seruminstitut Rabbit Cornea) Cells and Corneal Epithelial Cells from Rabbit Eyes. *Curr. Eye Res.* **2014**, *39*, 686−694.

(24) Tak, R. V.; Pal, D.; Gao, H.; Dey, S.; Mitra, A. K. Transport of Acyclovir Ester Prodrugs Through Rabbit Cornea and SIRC-Rabbit Corneal Epithelial Cell Line. *J. Pharm. Sci.* **2001**, *90*, 1505−1515.

(25) Takahashi, Y.; Koike, M.; Honda, H.; Ito, Y.; Sakaguchi, H.; Suzuki, H.; Nishiyama, N. Development of the Short Time Exposure (STE) Test: An in Vitro Eye Irritation Test Using SIRC Cells. *Toxicol. In Vitro* **2008**, *22*, 760−770.

(26) Shah, A.; Brugnano, J.; Sun, S.; Vase, A.; Orwin, E. The Development of a Tissue-Engineered Cornea: Biomaterials and Culture Methods. *Pediatr. Res.* **2008**, *63*, 535−544.

(27) Yang, R.; Wu, P.; Wang, X.; Liu, Z.; Zhang, C.; Shi, Y.; Zhang, F.; Zuo, B. A Novel Method to Prepare Tussah/ *Bombyx Mori* Silk Fibroin-Based Films. *RSC Adv.* **2018**, *8*, 22069−22077.

(28) Luangbudnark, W.; Viyoch, J.; Laupattarakasem, W.; Surakunprapha, P.; Laupattarakasem, P. Properties and Biocompatibility of Chitosan and Silk Fibroin Blend Films for Application in Skin Tissue Engineering. *Sci. World J.* **2012**, *2012*, 1−10.

(29) Jaramillo-Quiceno, N.; Álvarez-López, C.; Restrepo-Osorio, A. Structural and Thermal Properties of Silk Fibroin Films Obtained from Cocoon and Waste Silk Fibers as Raw Materials. *Procedia Eng.* **2017**, *200*, 384−388.

(30) Rajkhowa, R.; Levin, B.; Redmond, S. L.; Li, L. H.; Wang, L.; Kanwar, J. R.; Atlas, M. D.; Wang, X. Structure and Properties of Biomedical Films Prepared from Aqueous and Acidic Silk Fibroin Solutions. *J. Biomed. Mater. Res., Part A* **2011**, *97A*, 37−45.

(31) Yao, J.; Ohgo, K.; Sugino, R.; Kishore, R.; Asakura, T. Structural Analysis of *Bombyx Mori* Silk Fibroin Peptides with Formic Acid Treatment Using High-Resolution Solid-State ^{13} C NMR Spectroscopy. *Biomacromolecules* **2004**, *5*, 1763−1769.

(32) Ha, S.-W.; Tonelli, A. E.; Hudson, S. M. Structural Studies of *Bombyx m Ori* Silk Fibroin during Regeneration from Solutions and Wet Fiber Spinning. *Biomacromolecules* **2005**, *6*, 1722−1731.

(33) Liu, Q.; Wang, F.; Gu, Z.; Ma, Q.; Hu, X. Exploring the Structural Transformation Mechanism of Chinese and Thailand Silk

https://doi.org/10.1021/acsomega.2c01579
ACS Omega 2022, 7, 29634−29646

Fibroin Fibers and Formic-Acid Fabricated Silk Films. *Int. J. Mol. Sci.* **2018**, *19*, 3309.
(34) Qi, N.; Zhao, B.; Wang, S.-D.; Al-Deyab, S. S.; Zhang, K.-Q. Highly Flexible and Conductive Composite Films of Silk Fibroin and Silver Nanowires for Optoelectronic Devices. *RSC Adv.* **2015**, *5*, 50878−50882.
(35) Liu, J.; Chen, H.; Wang, Y.; Li, G.; Zheng, Z.; Kaplan, D. L.; Wang, X.; Wang, X. Flexible Water-Absorbing Silk-Fibroin Biomaterial Sponges with Unique Pore Structure for Tissue Engineering. *ACS Biomater. Sci. Eng.* **2020**, *6*, 1641−1649.
(36) Akturk, O.; Kismet, K.; Yasti, A. C.; Kuru, S.; Duymus, M. E.; Kaya, F.; Caydere, M.; Hucumenoglu, S.; Keskin, D. Wet Electrospun Silk Fibroin/Gold Nanoparticle 3D Matrices for Wound Healing Applications. *RSC Adv.* **2016**, *6*, 13234−13250.
(37) Hazra, S.; Nandi, S.; Naskar, D.; Guha, R.; Chowdhury, S.; Pradhan, N.; Kundu, S. C.; Konar, A. Non-Mulberry Silk Fibroin Biomaterial for Corneal Regeneration. *Sci. Rep.* **2016**, *6*, 21840.
(38) Liu, T.; Miao, J.; Sheng, W.; Xie, Y.; Huang, Q.; Shan, Y.; Yang, J. Cytocompatibility of Regenerated Silk Fibroin Film: A Medical Biomaterial Applicable to Wound Healing. *J. Zhejiang Univ., Sci., B* **2010**, *11*, 10−16.
(39) Kim, D. K.; Sim, B. R.; Khang, G. Nature-Derived Aloe Vera Gel Blended Silk Fibroin Film Scaffolds for Cornea Endothelial Cell Regeneration and Transplantation. *ACS Appl. Mater. Interfaces* **2016**, *8*, 15160−15168.

https://doi.org/10.1021/acsomega.2c01579
ACS Omega 2022, 7, 29634−29646